Biannual Open Access Journal
Peer-Reviewed/Refereed International Journal
JOURNAL OF GLOBAL RESOURCES
Published by: ISDESR, Jaipur, India

www.isdesr.org

ISSN: 2395-3160 (Print)
ISSN: 2455-2445 (Online)
July 2022, Volume 08 (02)
DOI Prefix: 10.46587/JGR

**05**

# SPATIAL RELATIONSHIP BETWEEN LAND-USE LAND COVER WITH SOIL EROSION IN THE NARMADA BASIN USING SENTINEL 2 IMAGE: ASSESSING THE PERFORMANCE OF RF MACHINE LEARNING CLASSIFIER

**Vinay Raikwar[1], Pramod Pagare[1]** and **Aminu Abdulwahab[2]**
[1]Dept. of Geography, Govt. Mahatma Gandhi Smrati PG College, Hoshangabad, MP, India
[2]Department of Natural Resources, TERI School of Advanced Studies, New Delhi, India
[2]Department of Surveying and Geoinformatics, Adamawa State, Nigeria
Email: vinay.utd@gmail.com

**How to cite this paper:**
Vinay Raikwara, Pramod Pagarea, Aminu Abdulwahab (2022) Spatial Relationship Between Land-Use Land Cover with Soil Erosion in the Narmada Basin Using Sentinel 2 Image: Assessing the Performance of RF Machine Learning Classifier, Journal of Global Resources, Vol. 08 (02)

**DOI:**
**10.46587/JGR.2022.v08i02.005**

**Received:** 15 May 2022
**Reviewed:** 25 May 2022
**Revised:** 05 June 2022
**Final Accepted:** 26 June 2022

OPEN ACCESS
Freely available Online
www.isdesr.org

**Abstract:** *In the past decades, increasing demand for cultivable soil, deforestation and land conversion in the region has led to severe soil and natural resources exhaustion. The grade and rate of the soil and land-use land-capacity connection has been determined using soil parameter data together with geographic information systems, utilizing machine learning methods (random forest).The analysis shows high and substantial land coverage over Grass Land area with 52,330.59 sq. km/54.5 percent, with an Urban growth of 19,255.36 sq.km/20.0 percent, 12,400.51 sq.km/12.9 percent for Agriculture, Forest land with 8,828.67 sq.km/9.2 percent, 1,970.382 sq.km/2.0 percent for water and the smallest land cover among the classes was cropland with 1,337.51 sq.km/1.4 percent area coverage. Random forest algorithms show that soil erosion for the whole Upper catchment was lower compared to the bottom catchment region and high soil erosion in line with the land conversation of natural vegetation. This analysis includes extra significant information and differences between kinds of land use soil erosion with a major and very severe area 38.337.55 sq.km / 39.9 percent; the severely eroded soil covers 29.346.59 sq.km / 30.5 percent; the modest soil erosion area (15.372.16 sq.km / 16.00 percent); the lowest or slightest soil erosion zone was 13066.73 sq.km/13.6 percent. To strengthen the status and use of the collected resources as a result of sustainable land use activities that benefit local rural life, inclusive and viable land use is needed immediately. The area where very severe soil erosion and the land cover has been correlated to determine the relationship with the existing land covers in the area, decreases of soil erosion indicates the change in the land uses. The correlation between the LULC and the soil erosion was 0.53, with an RMSE of 0.033 and a p-value of 0.000063.*

**Key words**: Spatial Relationship, Land-Use Land Cover, Soil Erosion, Narmada Basin

## Introduction

In many regions of the world, soil erosion is among the most significant soil degradations that cause environmental problems (Luetzenburg et al., 2020; Li et al., 2020). Soil erosion implies moving and conveying soil from numerous sources, including liquid, storm and movement of volume (Bullock, 2005). Land degradation is a significant type of erosion in wet and semi-damp climate areas, such as northern Iran "(Esmaeeli G. & Gholami, 2012; Khaleghi & Varvani, 2018)". Human activities may also lead to erosion by two means, directly by soil movement, such as the carriage, and indirectly by destabilizing slope materials, such as agriculture, and speeding up erosion by the wind, water or gravity. This eliminates land soil degradation by lowering agricultural productivity and plant loss in rainforests and fields, and it has significant ramifications for agriculture, food, and water supplies and leads to substantial repercussions of contamination and sedimentation of dam reservoirs on agriculture, food, and water resources "(Pierson et al., 2007; 2008; Gholami and Khaleghi, 2013; Akay et al., Aldrich et al., 2005;). Various variables effect soil erosion (Masson, 1971; Pastor and Castro, 1995; M. Kasasnovas, 1998), Di Stephano at al. (2000) and Uson (1998))" include precipitation amount/intensity. Pickup & M., (2000). Differing influences include the quantity and intensity of the precipitation. Several researches have been conducted on soil erosion. The soil erosion degree of Descroix and Poulenard (1995) was demonstrated (27 percent). Bohm & G., (1995) have showed the level of vegetation been highest than the soil and route gradient features. Kirkby et al. (2005) found that the slope-vegetation mix often impacts the hillside soil Erosion rate. Various methods are available on the hillside for monitoring soil erosion, soil erosion or runoff of certain precipitation events are estimated or within a certain period. The usage of the plots allows the exact time intervals to be chosen from a storm to a monthly or annually. Current care and recuperation are required for fields which make the process time consuming and expensive. Another possibility is the application of pins in erosion measurement, which were easier and more successful in prior studies. "Shumm and al, (1974); Shi et al. 9(2013); Haigh, (1978); (Boardman et al, 2015). (Chumm (1956); Emmett, (1964)". Sedimentary pins are cheaper and easier for users in comparison to field plots and are appropriate for large-scale applications such as an annual erosion rate. The use of erosion pins is therefore difficult in short-term estimates (e.g., a given precipitation, or a given day) (Ireland, 1939; Emmett, 1965; Haigh, 1977; Loughran, 1989; Hancock et al., 2008; Kearney et al., 2017 & Boardman and F., (2016)). Depending on the kind of erosion, actual accuracy and objective precision of measurement, the choice of methodology and strategy.

Several studies using erosion pins to measure various forms of ground erosion have been undertaken. "(Favis-Mortlock and B., 2016). Haigh (1977)" indicated that the usage of erosion pins was made in 1956 by Colbert (1956) and Schumm in the U.S. for the measuring of soil erosion. They employed erosion markers to calculate the rate of erosion in the Badlands. The riparian pines employed for erosion are also estimated to include riparian erosion (Lawler, 1978, 1991; 1992; 1993), lowlands (Streeter, 195; Summer, 1986) and Blackland erosion (Clarke, and Rendell, 2007; Nadal-Ronmero and others, 2011: Bardman et al., 2015; Hancock and Lowry, 15), and riparian erosion (2015). (Harvey,1974). Erosion pin is a powerful device for assessing hillside soil erosion in several case studies (Tervuren, 1990; Harden et al., 2009; Keay- Bright and Boardman, 2009). For example, in the Mediterranean Badlands, Nadal-Romero et al. (2011) employed and assessed several ways of monitoring sediments. Erosion pins were employed by Kumar Ghimire et al. (2011) to evaluate several forms of erosion in the Himalayas (E.g., erosion of the gullies, rill erosion, landslides and bank erosion). They showed that the Himalayan erosion rate in comparison to other places is notably high. Measurement of soils erosion is a costly and time-consuming operation that cannot be carried out across a large region of investigation. Field-based measuring models can be employed to resolve this problem. The purpose of these models is to relate the expected soil exposure (as source or as

endpoint) to the influence on the rest of the field of study and to the influence of soil erosion factors (for example, slopes, plant covers, soil characteristics) of the plot region or of the erosion pins. Therefore, methods including neural artificial networks (ANNs) and field information may reduce costs and workloads and allow us to predict the soil erosion process across the research region. ANN has been frequently employed in hydrological processes and environmental modelling "(Anctil and Rat, 2005; Isik et al., 2013; Gholami et al., 2018; Sahour et al., 2020; Alshehri et al., 2020)". The relationship between land use and soil usage and soil erosion, between policy-making trees and ANN was examined by Rosa et al. (1999). As a paradigm alternative to quantifiable, process-based erosion models for the South Downs of England, Harris and Boardman (1998) have employed expert systems in conjunction with the ANN. In addition, GIS would be a valuable mapping, analysis and severity for soil erosion, when associated with ANN's geographical information systems. This research seeks to analyse, depict/evaluate soil erosion and the link between land usage and land use by means of RF algorithms in the GIS mode in Google Earth and to identify the association between an area of soil erosion and a land cover in software R programming.

**Study Area**

The Narmada River is seventh biggest river with the Ganga, Brahmaputra, Godavari, Krishna, Indus, and Mahanadi being the only preceded by river network. Narmada River Basin (NRB) located in the Central Park of India with an area of the drainage area of 98,796 km2 at a mean altitude of 760 m between 72°32' E to 81°45' E Longitude and 21°20 N to 23°45' N Latitude. It has a length of 1312 km. The watershed area of the river encompasses the administrative states of Madhya Pradesh (86.18 percent), Gujarat (11.6 percent). Narmada and the Tapi Rivers, by contrast, flow westwards to the Arab Sea combined with other peninsular rivers that go into the Bay of Bengal in India (Godavari, Cauvery, Mahanadi). The river Narmada originates in the district of Amarkantak in the district of Anuppur and flows into the Bharuch, Arabian sea on the eastern coast (Fig. 1). At 1057 meters above sea level, it emerges from a small pond (Narmada Kund). The region is surrounded by northern Vindhyan, east by Maikala, south by Satpura and west by the Arabian Sea. The area is largely below the 500-meter-high normal sea level. On the left banks and on the right banks, on 19, the largest prosperity areas with a catchment area of approximately 3,500 sq.km are in Burhner, Banjar, Hiran Tawa, Chota Tawa, Orsang and Kundi

Approximately 35 percent of the territory in the basin lies in the forests and 60 percent in arable land, and 5 percent in pastures, wastelands, etc. The basin has a population of over 16 million people; however, the urban population is only around 20 percent of the total (CPCB, 1994). However, the major river banks on the left and right banks, with a catchment area of almost 3,500 km, are in Burhner, Banjar, Hiran Tawa, Chota Tawa, Orang and Kundi. In summer, temperatures vary between 40˚C and the 42˚C to the 8˚C and the 13˚C. In the summer (April to June) the evaporation rates are 6 mm to 28 mm and in winter (1 mm – 9 mm) (October to March). On the Narmada River and its tributaries, several dams have been erected. The basin is in operation with about 4,000 water-specific projects of different size and objectives. The important projects of the basin are "Bargi dam, Barna, Indra Sagar, Kolar, Omakareshwar, Maheshwar, Bhagwant Sagar, Tawa and Sardar Sarovar dam". The Sardar Sarovar Dam, has a height of 110.64 m and reservoirs of 3,700 ·106 $m^3$, is the biggest of the 29 big dams scheduled for Narmada.

Deccan Basalt, followed by the Vindhyan and Gondwana Groups is the principal lithological part of the basin. The meta group Bijawar, the small component contributing to basin geology is the gneissic complexes of the Archaean-Proterozoic period. The alluvium is primarily restricted to the Narmada valley. The river Narmada occupies a mega-tectonic zone of the sound line of Narmada and Tapi function. This area comprises multiple longitudinal,

faulty, vertical and lateral blocks with episodic history (Shankar 1991). Smectite clays with high hydraulic capacity are generally dark soils. In the upper basin, black soils are commonly mixed with sandy or laterite red soils. The soil profile is rather low and extends over the mountains and plateau. Red soils derive from the strong chemical weathering of basalt, leaching all the rock minerals except silica, iron and aluminium oxides. The soils demonstrate good drainage characteristics due to extensive leaching. The middle basin area Vindhyan and Satpura varies from shallow black grounds to medium black soils. The main soil types in the bottom part of the basin are black soils. On the other hand, the northern plateau contains black/red soils, Pliocene rocks and the latest alluvium characterize the Narmada basin (CWC 1996–99).

**Figure 01: Location of the Narmada River Basin in Central-Western India**

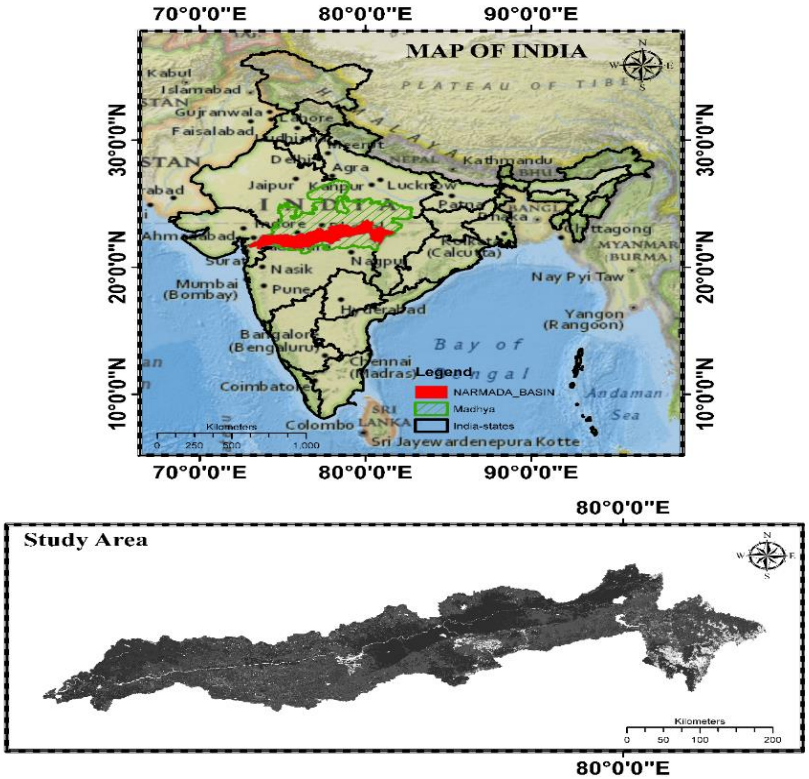


## Raster Image Acquisition and Pre-Processing

### Google Earth Engine (GEE)

The google earth engine (GEE) employs a multi-petabyte database of geospatial data and imaging satellites utilizing a planetary analytic capacity to make changes, map trends and quantify the variations on the earth's surface available and readily available for developers, scientists and researchers (Google Earth Engine Team). It is a tool to analyse geographical information utilizing a Python and JavaScript application programming interface (API). The approaches are developed here with JavaScript (Zeltner, 2016). A variety of data sets are displayed in the GEE data catalogue. The user gets access to imagery of the shuttle radar topography missions from several satellite image suppliers MODIS, LANDSAT, SENTINEL or digital elevation data (SRTM). Included in the GEE data catalogue are raw satellite data, Ortho-corrects, top-of-atmosphere and surface reflections (Gorelick et al., 2017).

### Satellite Data

GEE was used to acquire the sentinel 2 datasets ESA API Reflectance datasets for 2021 over part of the Narmada region. The code was configured to collect data over the region with a cloud cover condition of less than 10 percent as shown in figure (2). Also, the image was downloaded and exported to the drive and these image bands were further opened in Erdas Imagine for radiometric and atmospheric correction before the Random Forest (RF) land use and land cover classification using the coding in RStudio programming software.

**Figure 02: Sentinel 2 Image Collections with less than 10 percent Cloud effect from GEE, Atmospheric Correction**

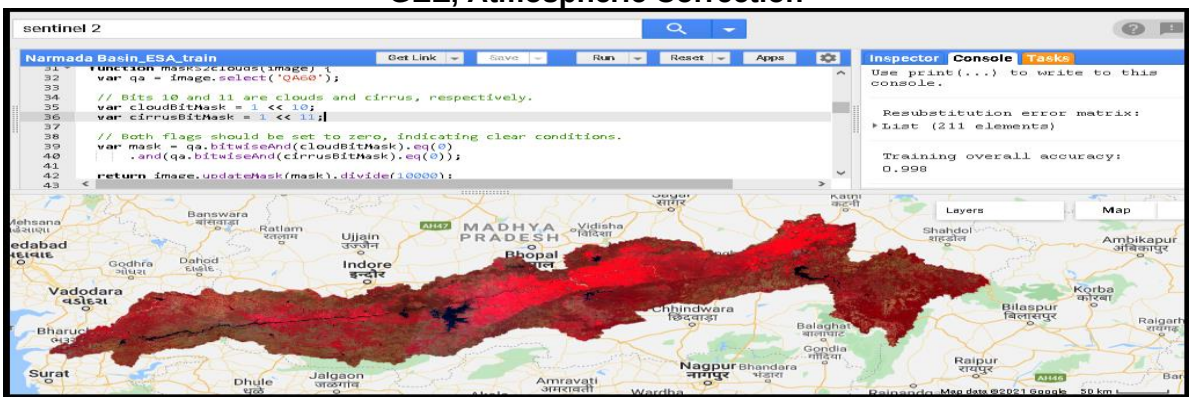


A great deal of research has been done on the issue of image correction for atmospheric effects. Those efforts lead to a range of atmospheric codes (models) of radiative transfer which can provide a practical assessment of the effects of atmospheric dispersion and absorption on satellite imagery. Once these effects have been detected for a particular imaging date, the effects of scattering and/or absorption may be removed in a band and/or pixel in the image, the image is then regarded as corrected against the atmospheric effects. The Erdas imagine was used for the analysis of the atmospheric effect on the downloaded Sentinel 2 datasets. The application of the atmospheric corrections module on the Erdas Imagine program eliminated any noise and haziness in the image. The final corrected image of 2021 was used in R studio for Random Forest (RF) classification algorithms and it was further exported to the ArcGIS for final graphical visualization.

**Random Forest**

Breiman's (2001) Random Forest RF is an ensemble training technique for enhancing regression/classification trees (CART) by the combination of several rule trees. For the most common class assignment to the input data, each tree contributes one vote. According to (Lin et al. 2010), the program benefits from two key strategies: the random selection and bagging of the subspace. First, RF builds several binary classification trees (tree) with many bootstrap samples by using original data to replace them. These trees contribute to the vote by units, and a majority vote is taken from all forest trees. The appropriate classification. Samples for the bootstrap are known as "out-of-bag." The OOB-sample may assess a misclassification error and variable significance (about 37 per cent of the entire data). Second, each node selects a number of input (tree) variables from a random sub-set of characteristics. This collection of qualities can be used for the optimal division. No cutting is undertaken and all forest trees have been maximized trees, to ensure that they are less similar or low distinctions “(Genuer, Poggi, and Tuleau-Malot 2010; Lin et al. 2010; Breiman 2001)”. To improve the precise categorization the RF parameters (i.e., mtree and ntree) must be defined “(Breiman 2001; Mutanga, Adam, and Cho 2012)”. The default numbers are 500, but the default value is 500 and the default value of the number of spectrum bands is 500. (m-try).Ideal combination of the two parameters was found by search strategy based on the OOB mistake estimation (Tian et al. 2009). The grid search value for mtree was between 1 and 5, with an interval of 500 varying in the grid search value for the ntree parameter between 500 and 10,000. A total of 100 ntree and mtree combinations were achieved during grid search. Image RF input was setup in the EnMAP box to identify Rapid Eye imagery for RF parameters (mtrees and ntrees) (Waske et al. 2012).

**Tuning of RF parameters**

The turning results show the lowest OOB error rate with the default mtree value of 0.14 in combination with the true value of 1000 (14 per cent). On the other side, with the combination of 6 mtree value with 800 ntree value, the greatest OOB error rate (6.4 per cent) was achieved.

The input parameters were selected to form the RF algorithm for classifying LULC classes, mtree value 4 and ntree value of 1000.

**LULC Categories Definition and Reference Data Collection**

The original classes of LULC were established based on the old existing Narmada LULC map created with Sentinel 2 and the NRSC LULC images from Atlas of India (and use land cover). The LULC categories were initially stratified using training datasets, which formed 6 spectral classes from seven inter-spectral strips on sentinel 2. Six spectral groups were then divided into all major LULC types (Table 1). A preceding field dataset for the LULC map of Narmada was created in 2021 based on a ground field data of the study area "(Lowry et al. 2007; Knorn et al. 2009)". Data were acquired for training and validation. The data was gathered by using a stratified random sample approach to sample LULC classes based on their representative size in the study region. Basic field tests were gathered via the research field of each class to find fields meeting the pre-selected homogenous content requirements of at least 20 $m^2$ (Lowry et al. 2007). The data was then randomly divided into training (70 per cent) and validation data sets (30 per cent). The training classification data collection (RF) is used to verify accuracy and to evaluate accurately the validation data set. With maximal optimisation, the RF settings have improved. (Duro, Dubé 2012 and Franklin, 2012).

**Annual Mapping of GIS soil Erosion Rate**

The RF and GIS algorithms were utilized for simulating and mapping annual rates of earth erosion according to the modelling method (training, cross-validation, and testing). The RF algorithm is the best model for the soil erosion network. Our approach included a connection between RF and GIS, which would identify soil erosion rates as well as the relationship to soil erosion over the research region. Inputs and erosion rates in a raster format were calculated and input and validated RF model was simulated the whole research region. Then simulated exposure rates in raster format were returned to the GIS to show the region of soil erosion and the rates of LULC. To verify the correctness of the mapping, we have compared the soil erosion levels of all validation pins to the corresponding simulated values in the final map. In GIS, DEM and the final map were created from the longitudinal patterns of the pitch analysed and annual erosion of the soil. The longitudinal profile throughout the research field was shown in fig. 3.

**Figure 03: Longitudinal Profile of the Narmada Basin**

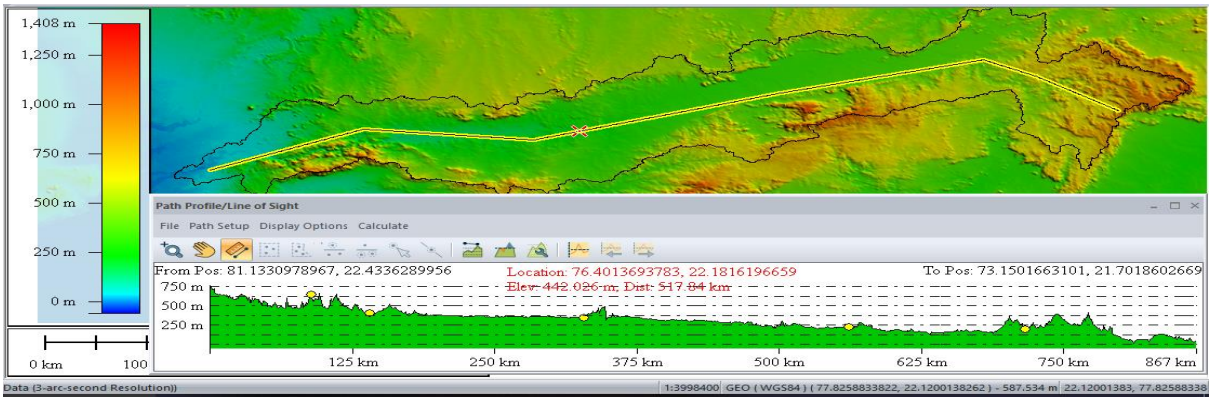


**Results**

**Soil Erosion Rate in the Narmada Catchment as affected by Land Use**

The erosion rate varied from 13.6 percent, 13066.73 sq.km to 39.9 percent in the whole Narmada basin and 38337.55 sq.km, respectively, for lower to higher areas. For the dominating terrain (flat to hilly landscape) the mean total value for the basin was (96123 sq.km) regarded quite high. One of the regions with substantially greater topographical features which concentrate runoff water producing serious soil erosion was the catchment studies. The study of the variance test shows that for the investigated region, the max (p-value < 0.05) coefficient of the variance is substantially higher (P-value < 0,05) for 2021. As large changes in LULC and

high rainfall erosion were the outcomes of climate change in recent years. The changes in soil loss and the distribution of water in LULC and climate are presented.

Climate change is having a major influence on rainfall distribution, affecting hydrological cessation of the watershed, including surface runoff, evapotranspiration of streams and loss of soil erosions (Neupane and Kumar, 2015). Mallick et al. (2014) and Mondal et al. (2017) have however said that LULC alterations with other variables, such as rainfall erosivity, land type, human ageing and so on, may result, from place to location and from time to time, in geographical variations in soil loss. The (Table 3) results indicate that there is a significant variation in cropland (1337.51 sq.km), and agricultural land (12400.51 sq. km, 12.9 per cent), between croplands and forest land with a high mean soil erosion (8828.67 sq.km, 9.2 per cent) with the forest area, which is in line with the finding of (Serpa et al. (2015)), which reported LULC change in soil erosions. Interestingly, high erosion levels similar to the robust countries of East Africa, such as Ethiopia, are also very important (Elias, 2017). This indicates the strong soil eroding and precipitation erosive variables faced with fast agricultural and industrial land conversions.

**Figure 04: Soil Erosion Map by RF Model**

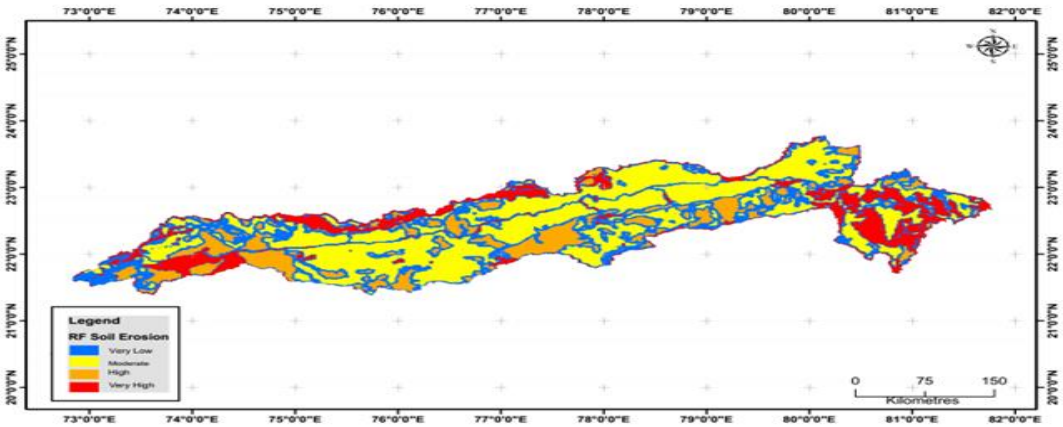


**Accuracy Assessment**

A separate test data set for both RF classifiers and detailed RF classification accuracy confusion matrices was used to evaluate the provision performance of the trained models. The RF classification was more precise. The RF's total accuracy was 99.2 percent, with a kappa of 0.96. All LULC classifications generally obtained an accuracy of more than 99 per cent, except cropland (CL) and grassland (GL, respectively), which had 89.0 percent and 88 percent. The RF classification has also been shown to be more than 98 per cent accurate for most LULC classes and the map results of the RF model are shown in figure 4. The mature cropland class was confused with grassland using this classification. In general, both RF LULC and soil erosion maps indicated the relationship between the two class areas and the soil erosion level within the research area (figure 5). The analogous areas collected by RF also confirm similar RF classifications. Between croplands, land and grassland there was confusion. The area of investigation is dominated by indigenous forests and grasslands, rocky soils and water basins. On the other side, settlements and coastal sand are less noticeable.

**LULC Classification RF Performance**

The application of RF resulted in six LULC classifications (Figure 3). As can be observed in the overall accuracy results, the LULC maps produced using both classifiers were not distinctly differentiated. The rocky shores pixels northeast of the maps showed a modest change (Figure 3). The method for RF classification measures the relevance of the variables in the classification process. The determination of the relevance of factors in this study enabled the identification of significance in the LULC categorization of each of Sentinel 2 bands (n = 5) (Figure 4). In the categorizing procedure, the Red Edges Belt is of major importance and

modelling accuracy in Sentinel 2 Band Assessment (n=5). The total accuracy of the LULC classification reduces by 1.4 percent, as seen in Figure 4, when the red band is omitted from the model. The infrared band is most beneficial in distinguishing bodies of water when the utility of every band for a particular category of LULC has been studied, whereas the blue band helps least in defining indigenous timber.

**Figure 05: Land use Land Cover Map by RF Model**

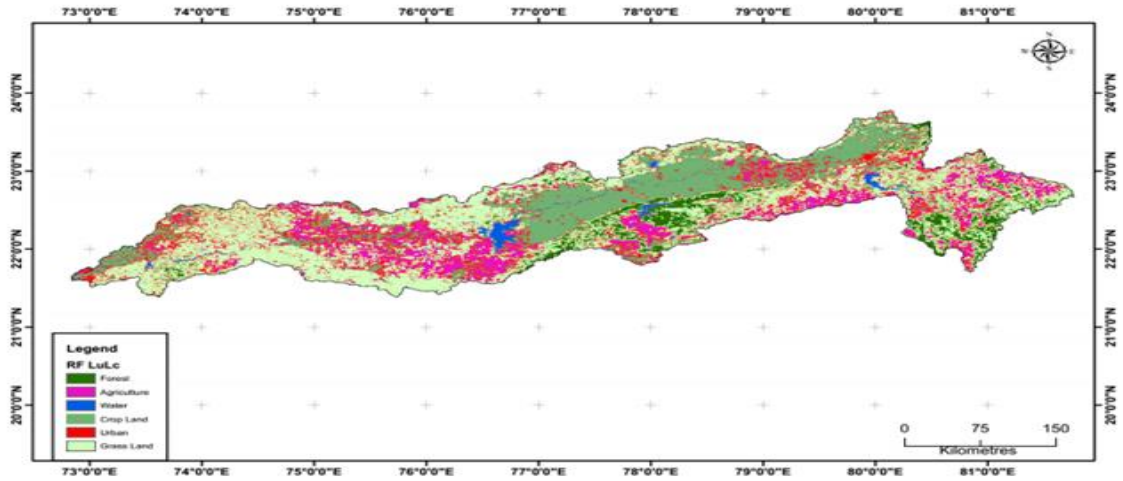


**Figure 06: Box Plot for Soil Erosion and LULC**

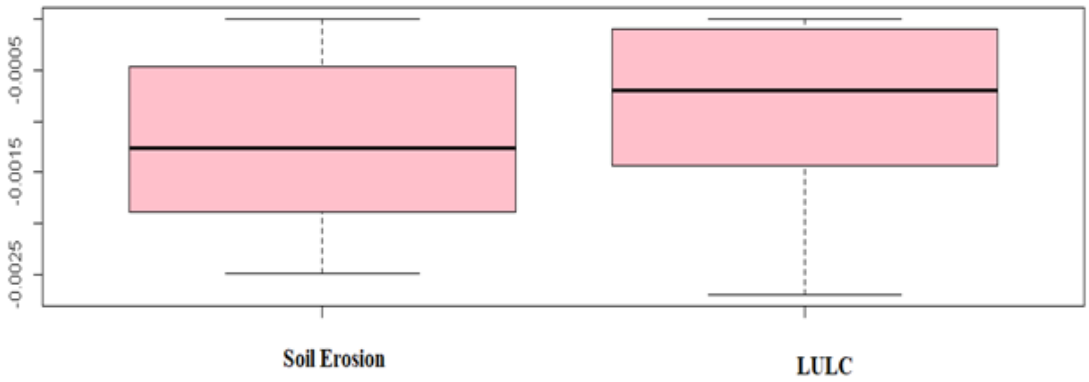


**Figure 07: Correlation Between Soil Erosion and LULC**

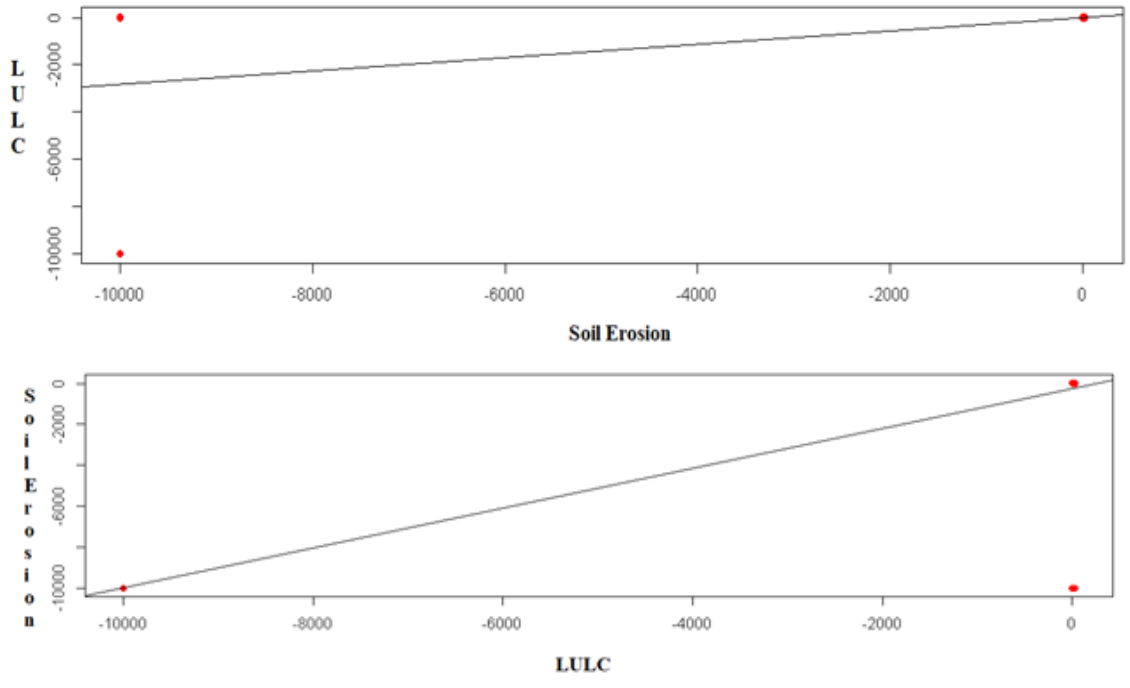

**Figure 08: Correlation Graph**


## Discussion

The recent past has accomplished many success stories in LULC mapping using several types of (fine, medium and coarse) spectral and spatial resolution for optical sensors. However, there are still questions about accuracy "(Foody 2002; Lu and Weng 2007)". Furthermore, the costs and availability of remotely sensed data with sufficient spatial, spectral and radiometric resolutions continue to hamper large LULC maps. The normal LULC maps produced by ordinary multi-spectral sensors (10m to 100m) are not sufficient for practical use (Foody 2002; Lu and Weng 2007). In contrast, fine-space resolution sensors (<5m) are limited by cost, availability, treatment, and a high level of data dimensions (Dalponte et al. 2009; Mutanga, Adam, and Cho, 2012). Locally constraints on remotely detected and medium-sized data limit the utilization and integration of field data with remotely sensed variables (Lu and Weng 2007). This study was intended in this context to evaluate the new-generation multi-spectral sensor performance (Sentinel 2).

The findings of the classification in this study showed that RF and classification images from Sentinel 2 is beneficial for mapping and comprehending complicated terrain. High classification precision was achieved using RF (Tables 2 and 3). Based on RF variable significance, the relevance of each Sentinel 2 band on classification output (Figure 4), which is a substantial contribution to the resolution of the error of classification commonly associated with multi-spectral usage, was further effectively identified using remotely sensed data (Foody 2002; Congalton and Green 2008; Congalton 1991; Oetter et al. 2001). RF was able to categorize the LULC classes stated above. The overall accuracies of RF and SVM were comparable. RF obtained more accuracy in categorization than around 1 percent. The Sentinel 2 data collection has the geographical and spectral properties that enable us to divide sugar cane regions into three LULC classes: mature, young and clear. In degraded grasslands and grasslands, we have effectively segregated sections covered by grass. In South Africa efforts have been unsuccessful to yet for the separation of such coverage groups using traditional multispectral information (SPOT and Landsat) (Fairbanks et al. 2000).

The accuracy of the class revealed that the accuracy of each grade was constantly increased. The tree classification combination in RF ensures that each classification determines the values of each sampled random vector. These random vectors have the same distribution for all forest classifications and each tree votes for one unit of the most popular input (Breiman 2001). This distribution and casting strengthen RF algorithms rather than noise and externalization (Watts et al. 2009). The high accuracy of classifications derived from this study gives trustworthy information on the numbers and scope of major land groups and may be used to evaluate agricultural production as well as ecosystem function, value, and productivity in terms of environmental deterioration.

Therefore, this knowledge is crucial in managing one of India's most precious ecosystems. However, these results can only be interpreted as initial as the additional study is required to expand the use of Sentinel 2 data to map LULC on different landscapes. Since high precision in large LULC classes has been achieved, further research has to be done to develop

a way to examine the lessons and detailed vegetation classes, because the red-edge band has the most significant influence. The considerable spectral variance in the same LULC class and the high spatial resolution on the red band resulted in an incorrect ranking specifically in the signal groups for vegetation. This calls for more study by evaluating the alternative way of classifying objects to deal with this challenge.

## Conclusion

This investigation assessed the capability to identify covers types in a heterogenous Narmada basin environment with a relatively new, spatial multispectral sensor, Sentinel 2, with a sophisticated RF classification algorithm. This work results in fresh insights into the performance of Sentinel 2 imaging by mapping an intricate environment with RF classifiers. The RF classification has been proven to have a considerable influence on all total classification and accuracy particularly in the vegetation zones. Comparing soil erosion with LULC, results showed that the RF LULC was comparable to that of soil erosion with R square 0.53 and a p-value of 0.000063 and RMSE of 0.033. The soil erosion was well defined. RF is a more robust approach that may be utilized for measuring and classifying variable relevance. It is straightforward to use because just two parameters must be optimised. In this investigation, errors in the spectrum variation assigned LULC classes in HR imagery may be ascribed as in previous relevant investigations. Therefore, alternative methodologies should be further studied, such as object classification.

## References


1. Akay, A.E., Erdas, O., Reis, M., Yuksel, A., (2008). Estimating sediment yield from a forest road network by using a sediment prediction model and GIS techniques. Build. Environ. 43, 687–695.
2. Aldrich, G.A., Tanaka, J.A., Adams, R.M., Buckhouse, J.C., (2005). Economics of western juniper control in central Oregon. Rangeland Ecol. Manage. 58, 542–552.
3. Anctil, F., Rat, A., (2005). Evaluation of neural networks streamflow forecasting on 47 watersheds. J. Hydrol. Eng. ASCE 10(1), 85-88.DOI: 10.1061/ (ASCE) 1084- 0699(2005)10:1(85).
4. Alshehri, F., Sultan, M., Karki, S., Alwagdani, E., Alsefry, S., Alharbi, H., Sahour, H., Sturchio, N., (2020). Mapping the Distribution of Shallow Groundwater Occurrences Using Remote Sensing-Based Statistical Modelling Over Southwest Saudi Arabia. Remote Sensing 12 (9), 1361.
5. Boardman, J., Favis-Mortlock, D., (2016). The use of erosion pins in geomorphology. Geomorphological Techniques, Chap. 3, Sec. 5.3.
6. Bullock, P., (2005). Climate change impact. Encyclopaedia of Soils in the Environment. Cranfield University–Silsoe, Silsoe, UK. 254-262. https://doi.org/10.1016/B0-12-348530-4/00089-8.
7. Bohm, P., Gerold, G., (1995). Pedo-hydrological and sediment responses to simulated rainfall on soils of the Konya Uplands (Turkey). Catena. 25 (1–41), 63–75.
8. Di Stefano, C., Ferro, V., Porto, P., Tusa, G., (2000). Slope curvature influence on soil erosion and deposition processes. Water Resour. Res. 36 (2), 607–617.
9. Dixon, B., (2004). Prediction of groundwater vulnerability using an integrated GIS-based neuro-fuzzy techniques. J. Spa. hydrol. 14 (12), 1–38.
10. Dixon, B., (2004). Prediction of groundwater vulnerability using an integrated GIS-based neuro-fuzy techniques. J. Spa. hydrol. 14 (12), 1–38.
11. Esmaeeli Gholzom, H., Gholami, V., (2012). A comparison between natural forests and reforested lands in terms of runoff generation potential and hydrologic response (case study: Kasilian Watershed). Soil Water Res. 4, 166–173.
12. Emmett, W.W., (1965). The Virgil Network: methods of measurement and a sampling of data collected. Int. Assoc. Sci. Hydrol. Publ. 66, 89–106.
13. Gholami, V., Booij, M.J., Tehrani, E.N., Hadian, M.A., (2018). Spatial soil erosion estimation using an artificial neural network (ANN) and field plot data. Catena. 163, 210–218.
14. Gholami, G., Khaleghi, M.R., (2013). The impact of vegetation on the bank erosion (case study: the Haraz River). Soil Water Res. 8 (4), 158–164.
15. Gholami, V., Booij, M.J., Tehrani, E.N., Hadian, M.A., (2018). Spatial soil erosion estimation using an artificial neural network (ANN) and field plot data. Catena. 163, 210–218.
16. Haigh, M.J., (1977). The use of erosion pins in the study of slope evolution. In, Shorter Technical Methods (ll). Technical Bulletin No. 18, British Geomorphological Research Group. Geo Abstracts: Norwich, UK;
17. Hancock, G.R., Loughran, R.J., Evans, K.G., Balog, R.M., (2008). Estimation of soil erosion using field and modelling approaches in an undisturbed Arnhem land catchment, Northern Territory, Australia. Geogr. Res. 46 (3), 333–349. https://doi.org/10.1111/ j.1745-5871.2008.00527.x.
18. Harvey, A.M., (1974). Gully erosion and sediment yield in the Howgill Fells, Westmorland. In: Gregory, K.J., Walling, D.E. (Eds.), Fluvial Processes in Instrumented Watersheds. Institute of British Geographers, London, pp. 45–58.

19. Harden, C.P., Foster, W., Morris, C., Chartrand, K.J., Henry, E., (2009). Rates and processes of streambank erosion in tributaries of the Little River, Tennessee. Phys. Geogr.
20. Harris, T.M., Boardman, J., (1998). Alternative approaches to soil erosion prediction and conservation using expert systems and neural networks. Modelling soil erosion by water. NATO ASI Series I, vol. 55. Springer-Verlag, Berlin, 461 – 477.
21. Isik, S., Kalin, L., Schoonover, J., Srivastava, P., Lockaby, B.G., (2013). Modelling effects of changing land use/cover on daily stream flow: An artificial neural network and curve number based hybrid approach. J. Hydrol. 485, 103–112.
22. Khaleghi, M.R., (2017). The influence of deforestation and anthropogenic activities on runoff generation. J. For. Sci. 63, 2017 (6): 245–253.
23. Khaleghi, M.R., Varvani, J., (2018). Simulation of relationship between river discharge and sediment yield in the semi-arid river watersheds. Acta Geophys. 66 (1), 109–119.
24. Khaleghi, M.R., Varvani, J., (2018). Simulation of relationship between river discharge and sediment yield in the semi-arid river watersheds. Acta Geophys. 66 (1), 109–119.
25. Kearney, P., Fonte, S.J., Garcia, E., Smukler, M., (2017). Improving the utility of erosion pins: absolute value of pin height change as an indicator of relative erosion. Catena. 163, 427–432. https://doi.org/10.1016/j.catena.2017.12.008.
26. Keay-Bright, J., Boardman, J., (2009). Evidence from field-based studies of rates of erosion on degraded land in the central Karoo, South Africa. Geomorphology 103, 455–465.
27. Kumar Ghimire, S., Higaki, D., Prasad Bhattarai, T., (2013). Estimation of soil erosion rates and eroded sediment in a degraded catchment of the Siwalik Hills. Nepal, Land 2, 370–391. https://doi.org/10.3390/land2030370.
28. Luetzenburg, G., Bittner, M.J., Calsamiglia, A., Renschler, CS., Estrany, J., Poeppl, R., (2020). Climate and land use change effects on soil erosion in two smalls agricultural catchment systems Fugnitz-Austria. Can Revull-Spain. Sci. Total Environ. 704, 135389. https://doi.org/10.1016/j.scitotenv.2019.135389.
29. Li, J., Ma, X., Zhang, C., (2020). Predicting the spatiotemporal variation in soil wind erosion across Central Asia in response to climate change in the 21st century. Sci. Total Environ. 709, 136060. https://doi.org/10.1016/j.scitotenv.2019.136060.
30. Loughran, R.J., (1989). The measurement of soil erosion. Prog. Phys. Geog. 13, 216–233.
31. Masson, J.M., (1971). L'érosion des sols par l'eau en climatméditerranéen. Méthodesexpérimentales pour l'étude des quantitésérodées 'al'échelle du champ. Thèse de Docteur-Ingénieur, USTL, Montpellier.
32. Martınez-Casasnovas, J.A., (1998). Soil-landscape-erosion. Gully erosion in the Alt Penedes-Anoia (Catalonia, Spain). A spatial information technology approach: spatial databases, GIS and remote sensing. Ph.D. Thesis. University of Lleida, Lleida, pp. 333 pp.
33. Nadal-Romero, E., Martinez-Murillo, J.F., Vanmaercke, M., Poesen, J., (2011). Scale-dependency of sediment yield from badland areas in Mediterranean environments. Prog. Phys. Geog. 35, 297–332.
34. Pierson, F.B., Batees, J.D., Svejcar, T.J., Hardegree, S.P., (2007). Runoff and erosion after cutting western juniper. Rangeland Ecol. Manage. 60, 285–292.
35. Pastor, M., Castro, J., (1995). Soil management systems and erosion. Olivae. 59, 64–74. Uson, A., (1998). Medidas de control de la erosion en suelos de vina de lascomarcasAnoia-AltPenedes (Barcelona). Efectividady viabilidad. Ph.D. Thesis. University of Lleida, Lleida.
36. Pickup, G., Marks, A., (2000). Identifying large-scale erosion and deposition processes from air bone gamma radiometrics and digital elevation models in a weathered landscape. Earth Surf. Proc. Land. 25.
37. Ranwell, D.S., (1964). Spartina salt marshes in southern England 11: Rate and seasonal pattern of sediment accretion. J. Ecol. 52, 79–94.
38. Rosa, D., de la Mayol, F., Lozano, S., (1999). An expert system/neural network model
39. (impelERO) for evaluating agricultural soil erosion in Andalucia region, southern Spain. Agri. Ecosyst. Environ. 73 (3), 211–226.
40. Rosas, M.A., Gutierrez, R.R., (2020). Assessing soil erosion risk at national scale in developing countries: The technical challenges, a proposed methodology, and a case history. Sci. Total Environ. 703, 135474. https://doi.org/10.1016/ j.scitotenv.2019
41. Schumm, S.A., (1956). Evolution of drainage systems and slopes in badlands at perth amboy, New Jersey. Geol. Soc. Am. Bull. 67, 597–646.
42. Sahour, H., Sultan, M., Vazifedan, M., Abdelmohsen, K., Karki, S., Yellich, J.A., Gebremichael, E., Alshehri, F., Elbayoumi, T.M., (2020). Statistical applications to downscale GRACE-Derived terrestrial water storage data and to fill temporal gaps. Remote Sens. 12, 533. https://doi.org/10.3390/rs12030533.
43. Tervuren, J.M., (1990). Soil loss by rain-wash: A case study from Rwanda. Z. Geomorphologie N.F.
44. Yair, A., Lavee, H., (1974). Areal contribution to runoff on scree slopes in an extreme arid environment. A simulated rainstorm experiments. Zeitschr, Fur Geom.
45. Zhao, Z., Chow, T.L., Rees, H.W., Yang, Q., Xing, Z., Meng, F.R., (2009). Predict soil texture distributions using an artificial neural network model. Comput. Electron. Agri. 65 (2009), 36–48.